Measurement of the neutral-current interactions of high-energy neutrinos and antineutrinos

P. Wanderer,* A. Benvenuti,† D. Cline, R. Imlay,‡ and D. D. Reeder
Department of Physics, University of Wisconsin, Madison, Wisconsin 53706

R. Stefanski
Fermi National Accelerator Laboratory, Batavia, Illinois 60510

C. Rubbia and L. Sulak
Department of Physics, Harvard University, Cambridge, Massachusetts 02138

F. Messing,§ W. T. Ford,‖ T. Y. Ling,¶ and A. K. Mann
Department of Physics, University of Pennsylvania, Philadelphia, Pennsylvania 19174
(Received 14 July 1977)

Measurements of the ν and $\bar{\nu}$ weak hadronic neutral-current total cross sections and hadron energy distributions are consistent with a $V-A$ form for this current. They are three standard deviations from pure V, pure A, or a pure T form and unambiguously exclude $V+A$ and any linear combination of S and P.

I. INTRODUCTION

The discovery of a class of neutrino interactions which yield no final-state charged lepton was first reported in 1973.[1] Since then, the initial observations of a weak neutral current have been confirmed by subsequent experiments which utilized neutrino and antineutrino beams covering a wide range of energies.[2-13] This paper gives a detailed account of our more recent measurements of neutral-current inelastic interactions of high-energy neutrinos and antineutrinos, which were briefly described earlier.[4] The measured ratio of the antineutrino and neutrino neutral-current total cross sections $\sigma_N^{\bar{\nu}}/\sigma_N^{\nu}$ and the measured hadron energy distributions are consistent with a V–A form for the neutral current and with the predictions of the gauge theories proposed by Weinberg and Salam[14] and others.[15] The results are three standard deviations from the pure forms V, A, or T, and unambiguously exclude $V+A$ and any linear combination of S and P. In most theories of the weak interaction, the presence of V, A interference implies a parity-violating component of the weak neutral current.

In Sec. II we describe the experimental apparatus including the characteristics of the several neutrino and antineutrino beams utilized. Following that we discuss the procedures for event selection (Sec. III) and various corrections to the data necessary to obtain $\sigma_N^{\bar{\nu}}/\sigma_N^{\nu}$ (Sec. IV). The implications of these results for the space-time structure of the weak neutral current are presented in Sec. V where other recent results are summarized. Conclusions are given in Sec. VI.

II. EXPERIMENTAL APPARATUS

The portion of the apparatus[16] which was used for identifying neutral-current interactions is shown in Fig. 1. Neutrinos, incident from the left, interact in a liquid-scintillator calorimeter. Muons are identified by their passage through iron absorbers, which filter out hadrons that do not interact in the liquid.

The calorimeter consists of 15 or 16 46-cm-thick modules, with dimensions transverse to the beam of 3.48 m × 2.87 m and a mass of 60 metric tons. The calorimeter measures hadron-shower energies E_H with a resolution of ~12% rms for $E_H > 20$ GeV, and with an ~15% rms resolution for lower values of E_H. The measured pion absorption length was 118 cm and the radiation length approximately 45 cm. The calorimeter is approximately an isoscalar target; the ratio of protons to neutrons is 1.32. Optical wide-gap spark chambers (WGSC), 2.8 m × 2.8 m in area, are placed after every fourth calorimeter module. These chambers, as well as those used to detect muons (see below), were photographed in two ±7.5° stereo views and in a 90° stereo view. In addition to the three views of the spark chambers, the information recorded for each event included the pulse height from each of the calorimeter modules and the timing and pulse height information from the scintillation counters. Typically 10^{13} protons were incident per machine cycle, producing one neutrino-induced event every two cycles.

Two muon detectors were used in the experiment. Detector $D1$ (Fig. 1) consisted of a 3.6 m × 3.6 m scintillation counter and a 2.8 m × 2.8 m spark

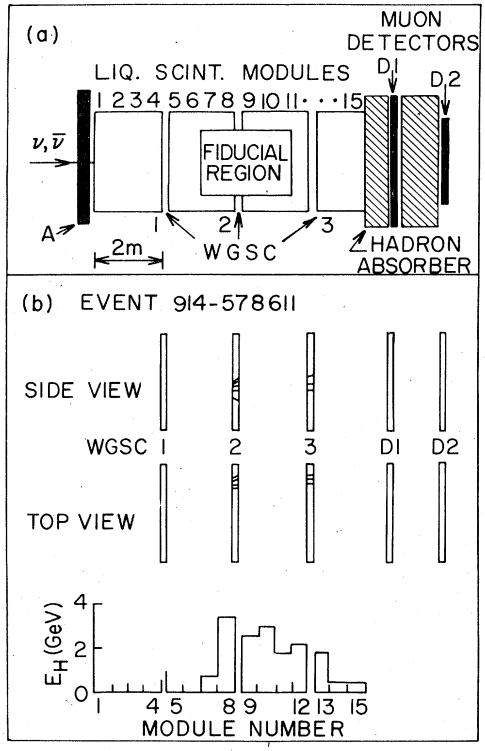

FIG. 1. (a) Schematic view of that portion of the target-detector used to identify neutral-current and charged-current neutrino interactions. Not shown are the remaining three sections of iron toroidal magnet. (b) Display of the calorimeter and spark-chamber information for a neutral-current event. The side view of the wide-gap spark chambers (WGSC) is from one of the 15° stereo views; the top view of the WGSC is from the 90° stereo view. The pulse heights in the calorimeter modules illustrate the development and absorption of the hadron shower, which had $E_H = 16.5$ GeV. (The gaps in the pulse-height distribution show the location of the WGSC.) No particles appear in D1 behind the hadron absorber.

chamber placed behind a 35 or 70 cm iron shield which absorbed most hadron showers. The counter was segmented with horizontal dividers into three equal sections, and the middle section was further segmented into four cells each 40 cm high. Detector $D2$ was a 2.8 m × 2.8 m spark chamber placed behind a 122-cm-thick iron toroid magnet which served as a further hadron shield. This magnet was the first of four used to measure muon momenta in charged-current interactions. Muons traversing $D1$ or $D2$ were detected with an efficiency >99%. However, muons were not detected if they were produced at too large an angle and thus missed the detector or if they had too low an energy to penetrate the hadron absorbers. Detector $D1$ had a very high muon acceptance (typically 95%), but a fraction of the events (typically 12%)

TABLE I. Relevant parameters for the four experiments reported here. The numbers of events have been corrected for muon detection efficiency and hadron punch-through. The parameter α, obtained from the measured CC events, indicates the composition of the beams.

Beam type	Length of beam gate	$\alpha \equiv \frac{N_{\mu^-}}{N_{\mu^-}+N_{\mu^+}}$	Number of events Neutral	Number of events Charged	Muon detection efficiency ϵ_μ Det. $D1$	Muon detection efficiency ϵ_μ Det. $D2$	Hadron-filter thickness (cm)	Hadron punch-through probability ϵ_p Det. $D1$	Hadron punch-through probability ϵ_p Det. $D2$	Fiducial volume Maximum $\lvert X\rvert, \lvert Y\rvert$ (cm)	Fiducial volume Z range (modules)
Horn	20 μsec	0.94	266	857	0.83	a	35	0.24	~0	120	5–12
QT 300	5 msec	0.83	158	599	0.84	a	35	0.20	~0	120	5–12
QT 380	5 msec	0.86	300	1042	0.95	0.84	70	0.12	~0	100	7–11
DH	20 μsec	0.27	69	198	0.94	0.79	70	0.07	~0	100	9–11

[a]Detector 2 had a different geometry for these experiments.

had hadrons which punched through the hadron absorber and were misidentified as muons. Detector $D2$ had a lower muon acceptance (typically 84%) but was essentially free of hadron contamination. Tests for possible systematic errors in the discrimination of neutral-current (NC) events from charged-current (CC) events were made by comparing the two detectors. The characteristics of the two muon detectors are listed in Table I.

Neutrino interactions which produced hadron showers with energy E_H greater than a preset minimum triggered the apparatus. This was the basic trigger for the experiment. The trigger efficiency was 99.5% for $E_H > 4$ GeV. Counter A was in anticoincidence to prevent triggers from incident charged particles. In order to monitor the E_H trigger, two other triggers were used. One was for muons which were produced by charged-current neutrino interactions in the calorimeter and which traversed all four sections of the iron toroidal magnet, and the other was for muons produced in the earth shield upstream of the apparatus. This latter trigger provided a continuous monitor of the calorimeter amplifier gains and of the optical system. During the time the beam was off, a gate 10% as long as the beam gate was opened in order to measure the background due to cosmic ray showers.

We report data taken with four different beams. They were a ν beam produced by 400-GeV protons with a horn focusing system (Horn),[13] ν beams produced by 300-GeV protons (QT 300) and by 380-GeV protons (QT 380) with a quadrupole triplet focusing system, and a $\bar{\nu}$ beam produced by 300-GeV protons with a two-horn focusing system and a plug to suppress high-momentum secondaries (DH).

III. EVENT SELECTION

Scanners were instructed to select photographs having at least two related tracks in the second or third spark chamber but no tracks in the first spark chamber (Fig. 1). The tracks in the spark chamber where the shower first appeared were projected back in order to determine the vertex of the interaction. The number of charged particles related to the shower was recorded for each spark chamber. Physicists scanned large portions of all four samples of data. The efficiency of the scanners was found to be 95%, and events missed by the scanners could not be correlated with any variable. The scanning inefficiency was independent of whether or not a muon was present in the muon detectors and independent of the position of the vertex and the hadronic energy of the event (for $E_H > 4$ GeV). In addition, a number of charged-current events were checked by an independent group of scanners. For this check, the transverse coordinates, X and Y, of event vertices were determined from extrapolation of the muon trajectories in the downstream spark chambers. The longitudinal (Z) position of the vertex was determined from the calorimeter pulse heights. The X and Y distributions obtained by the two methods were in good agreement, as shown in Fig. 2. We note also that Fig. 2 does not show a clustering of events about the edges of the detectors, as would be expected from backgrounds such as those due to neutrons incident from the side or neutrino interactions in the earth below and on the side of the calorimeter. The agreement between the two methods of determining event vertices limits such backgrounds to $\lesssim 1\%$ of the total number of events.

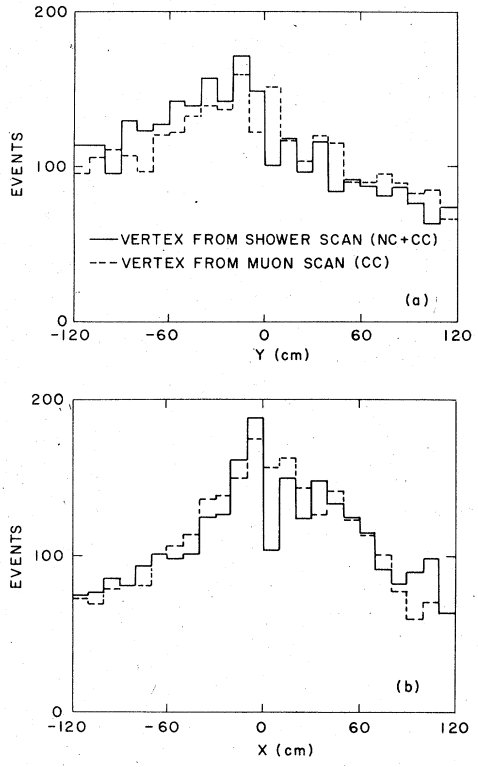

FIG. 2. The X and Y distributions of shower vertices as determined by the two methods discussed in the text. The distributions reflect the ~1 m radius of the ν beam and the position of the detector with respect to the beam.

After the visual and electronic information were combined, events were required to have vertices inside the fiducial volume. The criteria used to determine the fiducial volume were the muon detection efficiency and the hadron shower containment. For the high-statistics QT 380 data, the fiducial volume was chosen to be ±100 cm in both dimensions transverse to the beam, and calorimeter modules 7 through 11, as shown in Fig. 1.

Within this volume, the muon detection efficiency was everywhere calculated to be greater than 90%, as is discussed in Sec. IV A. Between two and four hadron absorption lengths were available for the measurement of E_H within this Z fiducial region. 80% of the energy of a hadronic cascade which has energy equal to the mean energy of the QT 380 data, 24 GeV, and which originates at the center of the longitudinal fiducial volume, $Z = 9$, is contained in the calorimeter. A correction was applied for energy in the hadron cascade which leaked out from the downstream end of the calorimeter.[16] The loss of energy out the sides was estimated to be ~10% for events occurring near the transverse boundary of the fiducial volume, 100 cm; no correction was made for this loss. Further discussion of hadron shower containment and corrections is in Ref. 16. The fiducial regions for all four data sets are given in Table I.

Initial event selection is made on the basis of visual criteria and it is therefore important to consider whether the selection procedure is biased toward neutral- or charged-current events. The distributions of the number of sparks in the spark chamber where an event was first observed are shown for neutral- and charged-current events in Fig. 3. (Charged-current events are taken to be those with a muon observed in Detector D1.) The distributions are very similar in shape. Differences could arise from different distributions in the variable $y \equiv E_H/E_\nu$ for neutral- and charged-current interactions, since the number of sparks is roughly correlated with E_H, or be due to scanning biases or spark-chamber inefficiency. A small difference is expected because each charged-current event has an extra track due to the departing muon. Thus charged-current events with one visible hadron satisfy the two-track requirement described earlier, but neutral-current events with one visible hadron do not. To correct for this bias, charged-current events with two tracks in the first spark chamber after the vertex were excluded from the data. Events with three or more tracks were not affected by this scanning bias. The cut removed 3% of the QT 380 data and 7% of the DH data. However, the cut does depend on E_H and for 4 GeV $< E_H <$ 10 GeV 10% of the QT 380 and 14% of the DH data were eliminated. Errors assigned to data in this E_H interval were increased to take account of the uncertainty due to this cut.

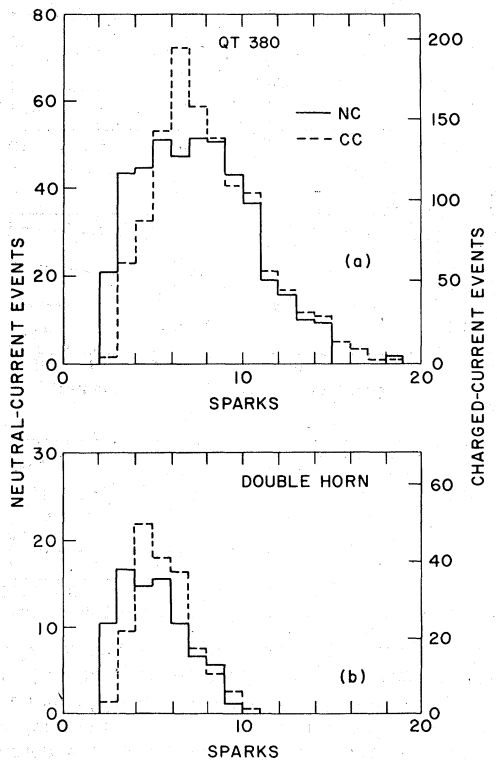

FIG. 3. Distribution of the number of sparks for neutral-current (NC) and charged-current (CC) events for two data sets, for events with $E_H > 4$ GeV. The vertical scales, which are different for NC and CC events, have been chosen so that the NC and CC histograms have equal areas.

As another test for possible biases in the visual criteria, an estimate of the quality of the hadron shower was made for each event selected. High-quality showers were those with well defined vertices. Events with large hadron energy had many sparks and well defined vertices; events with little hadron energy had fewer sparks and less well determined vertices. Also, lower-quality showers were more subject to backgrounds due to low-energy particles. It was found that the ratio of neutral current to charged-current events did not depend on the estimate of shower quality.

IV. CORRECTIONS TO THE DATA

A. Muon-acceptance calculation

Because of the choice of the small fiducial volume (~13% of the detector mass) and the large area and high efficiency of the muon identifiers, the acceptance of the apparatus for muons produced in charged-current events ϵ_μ was near unity. As a consequence, the calculated correction for undetected muons from these events was not particularly sensitive to the details of the neutrino beam spectra or to the detailed nature of the neutrino interaction.

Spectra for three of the neutrino beams are shown in Fig. 4. These spectra were calculated by Monte Carlo techniques based on measurements of π and K production[17] and on the properties of the hadron beam transport and focusing system.[18] The

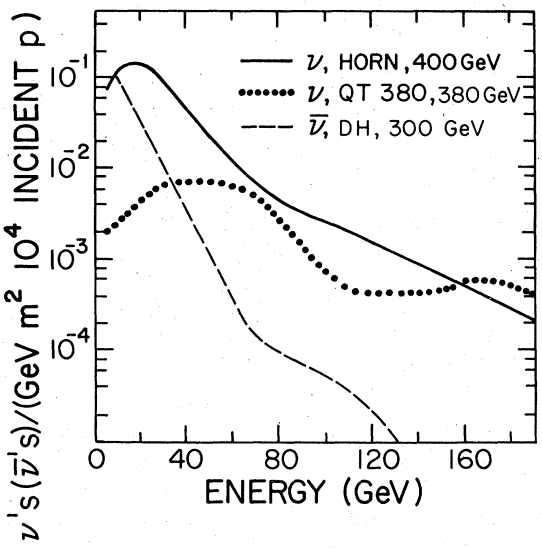

FIG. 4. Neutrino spectra for three of the beams used in the experiment. The spectrum of the QT 300 beam is similar in shape to that of the QT 380 beam but with lower average neutrino energy because the proton energy was 300 GeV.

relative ν and $\bar{\nu}$ content of the beams, given by the parameter

$$\alpha = \frac{\text{No. events with } \mu^-}{\text{No. events with } \mu^- + \text{No. events with } \mu^+}, \tag{1}$$

was determined from measurements of charged-current events and reflects the product of the flux and the cross section integrated over the spectrum of the incident beam.

The cross sections for charged-current interactions were measured previously with the same apparatus.[19] We write the differential cross sections for ν and $\bar{\nu}$ scattering in terms of the usual dimensionless scaling variables $x = q^2/2ME_H$ and $y = E_H/E_\nu$, with $q^2 = 2E_\nu E_\mu (1-\cos\theta_{\mu\nu})$. In the quark-parton model, with spin $-\frac{1}{2}$, isospin $-\frac{1}{2}$ partons, the high-energy cross sections for an isoscalar target assume the simple form[20]:

$$\text{for } \nu,\quad d^2\sigma/dxdy = \frac{G^2ME}{\pi}F_2(x) \times [a(x,E_\nu) + b(x,E_\nu)(1-y)^2], \tag{2}$$

$$\text{for } \bar{\nu},\quad d^2\sigma/dxdy = \frac{G^2ME}{\pi}F_2(x) \times [b(x,E_{\bar{\nu}}) + a(x,E_{\bar{\nu}})(1-y)^2], \tag{3}$$

where $a(x)$ and $b(x)$ can be interpreted as the fractions of quark and antiquark, respectively. Measurements of ν and $\bar{\nu}$ total cross sections near 1 GeV give

$$\langle b\rangle \equiv \int \bar{q}(x)dx \Big/ \int [q(x)+\bar{q}(x)]dx = 0.05 \pm 0.02,$$

where $q(x)$ and $\bar{q}(x)$ are the x distributions of quarks and antiquarks, respectively.[11] Our data[19] for $E_{\bar{\nu}} < 30$ GeV give 0.05 ± 0.05. In what follows we use the latter value for $E_{\bar{\nu}} < 30$ GeV and for all E_ν, which implies that $\langle a\rangle = 0.95$. We take $F_2(x)$ from our charged-current data.[21]

For $E_{\bar{\nu}} > 30$ GeV, where a significant scale breaking effect has been observed, [19] we again use empirically determined values of a and b.[22] The calculation of ϵ_μ is, however, relatively insensitive to this scale breaking effect because the average energy of the DH beam is close to the energy at which the onset of scale breaking takes place, and because in any case ϵ_μ is near unity. To show this, a calculation of ϵ_μ was made using the form of the

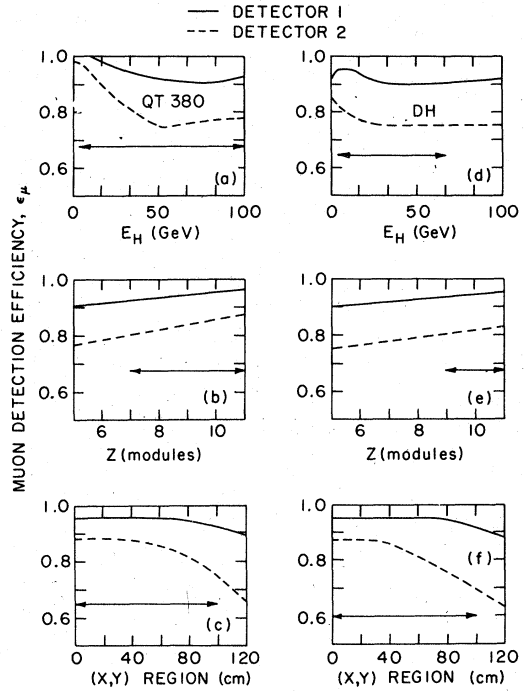

FIG. 5. Plots of the muon detection efficiency ϵ_μ for the QT 380 data [(a)–(c)] and the DH data [(d)–(f)] as functions of hadron energy E_H and the longitudinal and transverse positions of the interaction. In plotting the transverse position, the data are classified by defining a series of "square annuli" which cover the detector from the center out to 120 cm. Each "square annulus" is the region defined by the square $|X| < l_2$, $|Y| < l_2$, $|X| > l_1$, $|Y| > l_1$, where $l_2 - l_1 = 20$ cm, with l_2 in 20-cm steps. In each figure, arrows indicate the fiducial region.

$\bar{\nu}$ distribution in Eq. (3) with $\langle b\rangle = 0.05$ for all $E_{\bar{\nu}}$. This yielded for detector $D1$ a value of ϵ_μ 0.03 lower than the value $\epsilon_\mu = 0.94$ for the DH run.

The calculation of ϵ_μ takes into account the measured X, Y distributions of event vertices (Fig. 2), the beam spectra, muon ionization energy loss, resolution in the E_H measurement, and the magnetic field in the iron toroid. Events were assumed to be uniformly distributed along the beam axis. The values of ϵ_μ for the QT 380 data and the DH data are shown as functions of the space coordinates and E_H in Fig. 5. The average values of ϵ_μ for each of the four sets of data are given in Table I. Generally speaking, the loss of muons due to the finite angular acceptance of the detector was greater than the loss due to muons ranging out in the detector or in the hadron absorber.

B. Hadron punch-through

Energetic hadrons from neutral-current interactions which penetrate the hadron filter will simulate charged-currents events. For $D2$, located behind >17 collision lengths of absorber, the punch-through probability ϵ_p was negligible. The values of ϵ_p for $D1$, located behind >5 collision lengths, were ~12% averaged over the detector and the E_H spectrum for the QT 380 data. To correct for this misidentification, values of ϵ_p for $D1$ were measured using charged-current events which had a muon identified in $D2$. Correcting for δ rays,[23] ϵ_p was the fraction of such events which had more than one particle in $D1$. Plots of ϵ_p for the QT 380 data are shown in Fig. 6, where the attenuation length of the hadron shower is seen to be in agreement with our measured pion absorption length. These values of ϵ_p, measured for a 70-cm-thick hadron absorber, are consistent with those measured for the QT 300 and Horn runs, where the hadron absorber was 35 cm thick, when allowence is made for the difference in thickness. The average value of ϵ_p for each of the four data sets is given in Table I.[24]

For the Horn data, a second procedure was used to check the punch-through correction made by the method discussed above.[13] The difference between the track direction observed in the $D1$ spark chamber and the direction specified by a line from the event vertex to the position of the track in the $D1$ spark chamber was determined. From a sample of

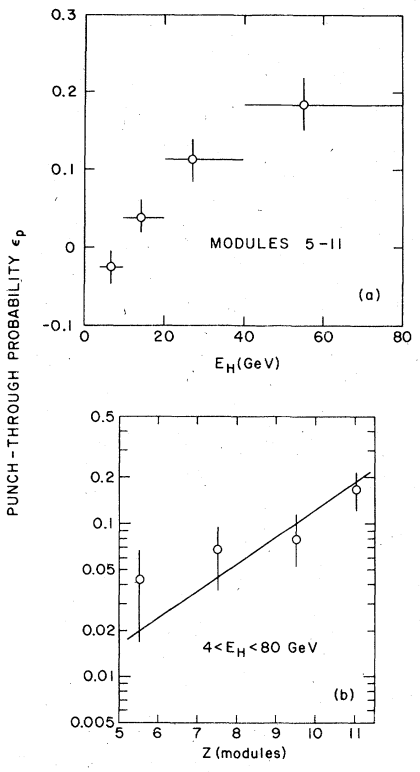

FIG. 6. The probability that hadrons will be observed in D1, ϵ_p, is plotted versus (a) E_H and (b) Z (calorimeter module). The straight line illustrates a pion attenuation length of 118 cm.

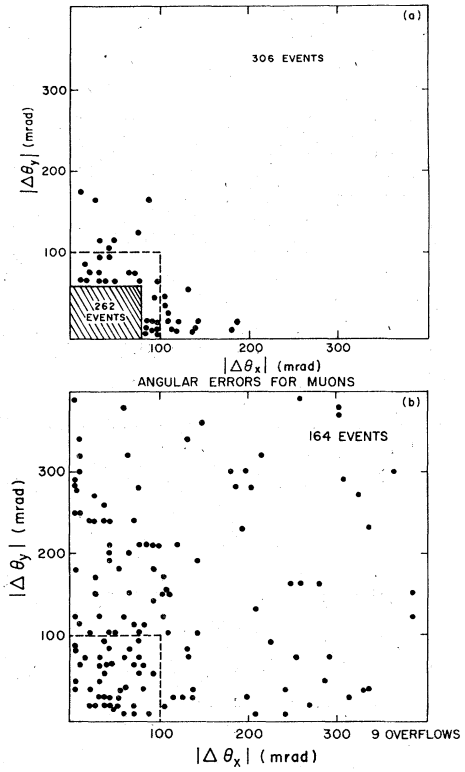

FIG. 7. Measured angular errors in the Y-Z plane ($\Delta\theta_y$) and in the X-Z plane ($\Delta\theta_x$) for (a) muon tracks and (b) hadron tracks measured in the D1 spark chamber.

charged-current events, it was found that for 93% ± 2% of the muons the difference of the angles was <100 mrad, while only 24% ± 4% of the hadrons had angle differences less than this (Fig. 7). Thus measurement of the corresponding difference of angles for neutral-current-event candidates discriminated between muons and hadrons in $D1$ and allowed hadron punch-through to be removed in a statistical way. This procedure was carried out for cuts at 100 and 60 mrad and both gave punch-through corrections that agreed well with those based on ϵ_p.

Rather than make a large correction for hadron punch through for events with $E_H > 100$ GeV, such events were excluded from the QT 380 data. The determination of the neutral current to charged-current cross-section ratio is nearly insensitive to this cut because the events with $E_H > 100$ GeV were only 10% of the data and because they had approximately the same neutral-current to charged-current ratio as events with lower E_H. For similar reasons, events from the QT 300 run with $E_H > 40$ GeV (25% of the total) were excluded. The horn and DH runs, with lower beam energies, were not affected by this cut.

C. Corrections and checks

The observed ratio of neutral-current to charged-current events,

$$R_{\text{raw}} = \frac{\text{number of events with no detected muon}}{\text{number of events with a detected muon}}, \tag{4}$$

was corrected for the effects of muon acceptance and hadron punch-through with the formula

$$R = \frac{(\epsilon_\mu + \epsilon_p - \epsilon_\mu \epsilon_p)(1 + R_{\text{raw}}) - 1}{1 - \epsilon_p (1 + R_{\text{raw}})} . \tag{5}$$

R_{raw} shows significant variation with vertex location due to changes in muon acceptance and hadron punch-through as exhibited in the largest sample, the QT 380 data, shown in Figs. 8(a) and 9(a). After correction, R is approximately constant as a function of vertex position and is the same for both detectors [Figs. 8(b) and 9(b)]. Similar plots for the other three data sets also show R to be constant as a function of vertex position; the DH data are shown in Fig. 10. The uniformity of R versus vertex position indicates that the corrections have been applied correctly and shows no evidence for a serious contamination of the neutral-current sample.

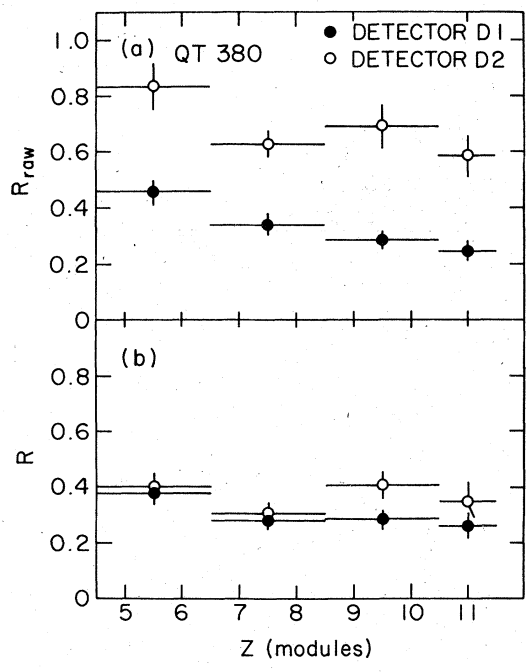

FIG. 8. The ratios of neutral-current events to charged-current events for the QT 380 data (a) R_{raw} and (b) R, as defined in the text, are plotted against longitudinal position (calorimeter module number).

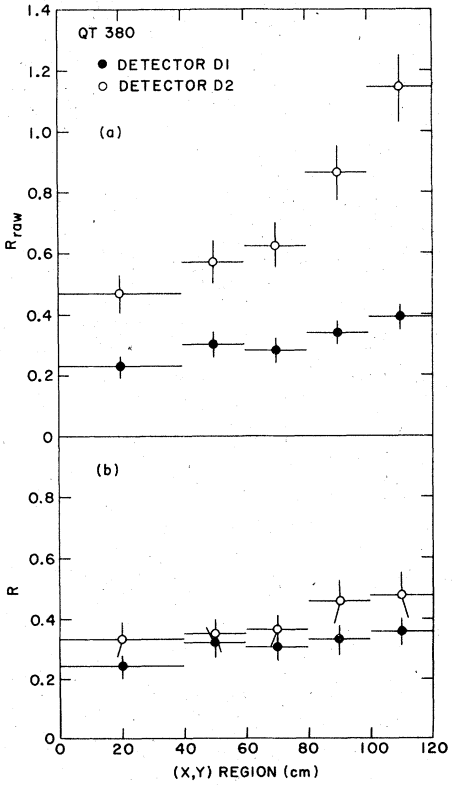

FIG. 9. The ratios of neutral-current events to charged-current events for the QT 380 data (a) R_{raw} and (b) R, as defined in the text, are plotted against transverse position ("region" is defined in Fig. 5).

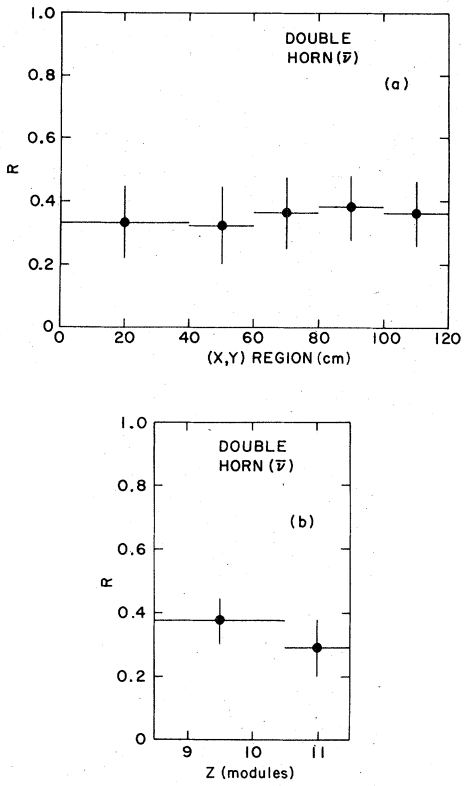

FIG. 10. The corrected ratio of neutral-current events to charged-current events R, defined in the text, is plotted against (a) transverse position and (b) longitudinal position for the DH data.

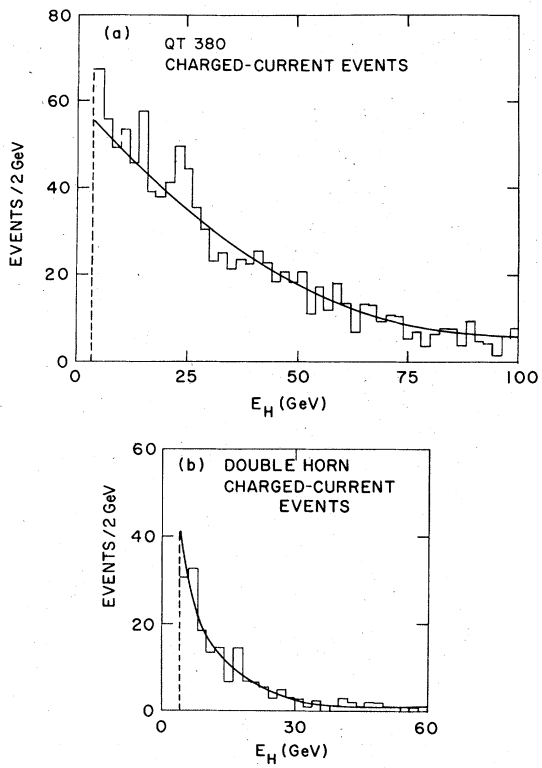

FIG. 11. Comparison between the calculated and measured hadron energy distributions for charged-current events for (a) the QT 380 data and (b) the DH data. The calculation, shown by the solid line, has been normalized to give the number of events in the histogram.

The values of R determined from Eq. (5) are relatively insensitive to errors in ϵ_μ and ϵ_p. For example, the QT 380 data had $\langle\epsilon_p\rangle=0.12$, $\langle\epsilon_\mu\rangle=0.95$. If the punch-through ϵ_p or the fraction of muons which are missed, $1-\epsilon_\mu$, are changed by 25% (i.e., $\langle\epsilon_p\rangle=0.15$, $\langle\epsilon_\mu\rangle=0.94$), the value of R, 0.30 changes by 6% (~0.02).

A further independent check on the corrections is made by comparing the calculated and measured E_H distributions of events with visible muons in Fig. 11, where the data are seen to be consistent with the calculation.

D. Background due to ν_e interactions

The interactions of electron-type neutrinos simulate neutral-current events in our apparatus. The ν_e background was calculated directly from the ν_μ spectrum using the ratio of production cross sections, branching fractions, and phase space for pion and kaon decays which yield ν_e and ν_μ.[18] For both the QT 380 and the DH beams, the background in the measurement of the total cross sections is ~0.5%. A 3% correction was made to the QT 380 data at the highest E_H.

E. Background due to cosmic rays

The scan of the QT 380 data, the largest of the four samples reported here, found no events which occurred during the cosmic ray gate, while finding ~2000 beam-related events. This places a limit of 0.5% on the cosmic ray background.

V. EXPERIMENTAL RESULTS

The data can be used to determine the space-time structure of the weak neutral current in two ways. First, we obtain the total-cross-section ratio for neutral currents $\sigma_N^{\bar{\nu}}/\sigma_N^{\nu}$, from the measured values of R for ν and $\bar{\nu}$. This cross-section ratio will be unity if the neutral current has one of the pure forms V, A, or T, or is any linear combination of S and P, since then no interference terms that change sign under the interchange of neutrino and antineutrino are present in the expressions for the ν and $\bar{\nu}$ cross sections. If different than unity, the cross-section ratio can be used to determine the mixture of currents present. Second, the inelasticity ($y\equiv E_H/E_\nu$) distribution for neutral-current interactions is related to the di-

rectly measured distribution in E_H. In the quark-parton model, the y distributions for any combination of V and A currents will have the forms[25]

$$\frac{1}{E}\frac{d\sigma_N^{\nu}}{dy} = \text{const}[a + b(1-y)^2],$$
$$\frac{1}{E}\frac{d\sigma_N^{\bar{\nu}}}{dy} = \text{const}[b + a(1-y)^2], \tag{6}$$

where E is the neutrino energy and a and b are the relative fractions of quarks and (nonstrange) antiquarks, respectively ($a+b=1$). The y distribution for any mixture of V and A currents can be duplicated by some combination of S, P, and T interactions. Nonetheless, specific combinations of S, P, and T interactions can be tested. The y distribution for any mixture of S and P currents is the same for ν and $\bar{\nu}$:

$$\frac{1}{E}\frac{d\sigma}{dy} = \text{const} \times y^2 . \tag{7}$$

For a pure T neutral current, the y distribution is also identical for ν and $\bar{\nu}$:

$$\frac{1}{E}\frac{d\sigma}{dy} = \text{const} \times (1 - \tfrac{1}{2}y)^2 . \tag{8}$$

Interference terms between T and S, P currents will have the form $y(2-y)$.

A. Total cross sections

The ratio R_{raw} for each data set was corrected for hadron punch-through and muon acceptance to yield

$$R = \sigma_N(E_H > 4 \text{ GeV})/\sigma_C(E_H > 4 \text{ GeV}) . \tag{9}$$

The corrected ratio R is related to the neutral current to charged current ratios for ν and $\bar{\nu}$, R^{ν} and $R^{\bar{\nu}}$, by the parameter α [Eq. (1)], which gives the $\nu(\bar{\nu})$ contamination of the $\bar{\nu}(\nu)$ beams:

$$R = \alpha R^{\nu} + (1-\alpha)R^{\bar{\nu}} . \tag{10}$$

The values of R^{ν} and $R^{\bar{\nu}}$ determined from the four samples of data are given in Table II.

The errors assigned to the values of R^{ν} and $R^{\bar{\nu}}$ in Table II include both statistical and systematic uncertainties. The statistical errors are ±0.020 on R^{ν} as determined from the QT 380 data and ±0.055 on $R^{\bar{\nu}}$. For the QT 380 data, the contributions to the error in R^{ν} due to uncertainty in ϵ_{μ} and ϵ_{p} were each taken as ±0.02. They were estimated by varying the charged-current model and the form on the punch-through. An additional ±0.02 was allowed for other sources of error. The same systematic errors were assigned to $R^{\bar{\nu}}$, except that the error due to uncertainty in ϵ_{μ} was estimated to be ±0.03 because of the relatively larger uncertainty in the form of the antineutrino charged-current cross sections. An additional uncertainty is present in the DH data relative to the QT 380 data because the DH antineutrino spectrum has a lower mean energy and a smaller average inelasticity y, making event recognition more difficult and increasing the importance of the 4-GeV E_H cut. A conservative estimate of ±0.07 was made for this added uncertainty.

TABLE II. The values of R^{ν} or $R^{\bar{\nu}}$ for $E_H > 4$ GeV. The errors assigned to R^{ν} and $R^{\bar{\nu}}$ include both statistical and systematic effects.

Beam type	R^{ν} ($E_H > 4$)	$R^{\bar{\nu}}$ ($E_H > 4$)	Comment
Horn	0.31 ± 0.06		Pure ν beam, $\langle E_{\nu}\rangle = 53$ GeV
QT 300	0.24 ± 0.06		Mixed beam, $\langle E_{\nu}\rangle = 78$ GeV
QT 380	0.29 ± 0.04		Mixed beam, $\langle E_{\nu}\rangle = 85$ GeV
DH		0.39 ± 0.10	Pure $\bar{\nu}$ beam, $\langle E_{\bar{\nu}}\rangle = 41$ GeV

Previously, we reported[3] the values $R^{\nu} = 0.11 \pm 0.05$ and $R^{\bar{\nu}} = 0.32 \pm 0.09$, both for $E_H > 4$ GeV. The difference between the earlier value of R^{ν} and the values given in Table II is due to the difficulty of the method used to extract R^{ν} and $R^{\bar{\nu}}$ from the first data samples. In the two most recent runs, QT 380 and DH, the corrections to the data have been appreciably reduced relative to the data reported earlier. The fraction of unseen muons is lower by a factor of two (4% to 5%, versus 9%), largely due to the choice of a smaller fiducial region (100 cm × 100 cm, versus 120 cm × 120 cm). The hadron punch-through has also been reduced by a factor of two, from 24% to 12%, due to a doubling of the hadron absorber thickness. Overall, the consistency of the values of R^{ν} obtained from the Horn, QT 300, and QT 380 runs, which have significantly different fiducial volumes and hadron absorbers, argues against gross errors in the determination of ϵ_{μ} and ϵ_{p}. Further, we estimate that the systematic uncertainties due to these corrections are correspondingly smaller in the QT 380 and DH data than in the data previously published. Finally, the systematic uncertainties in the film scanning are also reduced because the hadron showers produced by the QT 380 beam ($\langle E_{\nu}\rangle = 85$ GeV) have higher energy and are thus easier to recognize than the showers of the previous data ($\langle E_{\nu}\rangle = 53$ GeV).

Generally, it is not possible to obtain the ratio of the total cross sections $\sigma_N^{\bar{\nu}}/\sigma_N^{\nu}$ from

$$\sigma_N^{\bar{\nu}}(E_H > 4)/\ \sigma_N^{\nu}(E_H > 4)$$

in a way that is independent of a model of the space-time structure of the neutral current. However, model-independent limits on $\sigma_N^{\bar{\nu}}/\sigma_N^{\nu}$ can be obtained. If the neutral current has exactly the same space-time structure as the charged current, the ratios R^{ν} and $R^{\bar{\nu}}$ will not depend on the cut $E_H > 4$, since the y distributions for both neutral- and charged-current interactions are the same.[26] The inequality $R^{\nu}(E_H > 0) \geq R^{\nu}(E_H > 4)$ will obtain for any V, A combination for the neutral current if the charged current is close to $V-A$. This result is a consequence of the fact that the distribution dN/dy is constant in y for $V-A$. Admixing the form $V+A$ introduces a $(1-y)^2$ component to the neutrino distribution, and forces proportionately more events to have lower E_H. Similarly, $R^{\bar{\nu}}(E_H > 0) \leq R^{\bar{\nu}}(E_H > 4)$. The antiquark content of roughly 5% does not change the inequality.

The ratio $\sigma_N^{\bar{\nu}}/\sigma_N^{\nu}$ may be calculated from R^{ν}, $R^{\bar{\nu}}$ (for $E_H > 0$) and the measured ratio of the charged-current cross sections for neutrinos and antineutrinos with the relation $\sigma_N^{\bar{\nu}}/\sigma_N^{\nu} = (R^{\bar{\nu}}/R^{\nu})(\sigma_C^{\bar{\nu}}/\sigma_C^{\nu})$. Since the ratio of the charged-current cross sections is changing with energy,[19] it is necessary to specify the energy at which the calculation is made. Noting from Table II that R^{ν} is approximately constant over the average energy interval from 53 to 85 GeV, and that it is the same as that obtained by the Gargamelle experiment[11] for $E_{\nu} \sim 1$ GeV, we take that same value of R^{ν} at 41 GeV, the average energy of the DH beam used to obtain $R^{\bar{\nu}}$. At 41 GeV we calculate the inequality

$$\frac{\sigma_N^{\bar{\nu}}}{\sigma_N^{\nu}} \leq \frac{R^{\bar{\nu}}}{R^{\nu}} \frac{\sigma_C^{\bar{\nu}}}{\sigma_C^{\nu}} = \left(\frac{0.39 \pm 0.10}{0.29 \pm 0.04}\right)(0.45 \pm 0.08)\,,$$
$$\frac{\sigma_N^{\bar{\nu}}}{\sigma_N^{\nu}} \leq 0.61 \pm 0.25\,, \tag{11}$$

where the ratio $\sigma_C^{\bar{\nu}}/\sigma_C^{\nu}$ is obtained from earlier measurement.[19]

To obtain $\sigma_N^{\bar{\nu}}/\sigma_N^{\nu}$, rather than its upper limit, it is necessary to correct for events with $E_H < 4$ GeV. We test possible forms for the weak neutral current by using the assumed form to correct the data for missing events and then comparing the values for $\sigma_N^{\bar{\nu}}/\sigma_N^{\nu}$ so obtained with the values expected for that form. Because of the high energy of the neutrino beams, the fraction of neutrino events with $E_H < 4$ GeV is small (~7%). Thus, for any combination of V and A currents [any value of the coefficient a in Eq. (6)], the difference between $R^{\nu}(E_H > 0)$ and the measured value $R^{\nu}(E_H > 4)$ is negligible within experimental error. The ratio $R^{\bar{\nu}}$ is more sensitive to the exact form of the interaction because the average antineutrino beam energy is lower. For various forms of the weak neutral current given in Table III, the corrected, experimental values of $\sigma_N^{\bar{\nu}}/\sigma_N^{\nu}$ are compared with the expected values for this ratio. From Table III, S, P, and $(V+A)$ forms are clearly ruled out. The experimental value of $\sigma_N^{\bar{\nu}}/\sigma_N^{\nu}$ for pure V, A, or T is three standard deviations away from the expected value but is within one standard deviation of the value expected for $V-A$.

We obtain the best fit for the space-time structure of the neutral current by using the general forms of the $y \equiv E_H/E_{\nu}$ distribution given in Eq. (6). For a $V-A$ interaction $a \approx 1$ and $b \approx 0$, while pure V or pure A require $a = b = \frac{1}{2}$. The best fit is obtained by varying a and b until the expected value of $\sigma_N^{\bar{\nu}}/\sigma_N^{\nu}$ agrees with the corrected experimental value. For the best fit, $\sigma_N^{\bar{\nu}}/\sigma_N^{\nu} = 0.48 \pm 0.20$, $a = 0.85 \pm 0.12$, $b = 0.15 \pm 0.12$. This gives the equivalent forms for the weak neutral current: $A - (0.7 \pm 0.3)\,V$ or $V - (0.7 \pm 0.3)\,A$.[27] The total-cross-section ratios are then

$$R^{\nu}(E_H > 0) \equiv \sigma_N^{\nu}/\sigma_C^{\nu} = 0.30 \pm 0.04\,,$$

TABLE III. The measured values of $\sigma_N^{\bar{\nu}}/\sigma_N^{\nu}$, after correction for the loss of events with $E_H < 4$ GeV according to the form of the weak neutral current in the first column. The corresponding values of $\sigma_N^{\bar{\nu}}/\sigma_N^{\nu}$, expected from theory, are given in column three. An antiquark contribution of 5% has been assumed.

Form of the weak neutral current	$\sigma_N^{\bar{\nu}}/\sigma_N^{\nu}$ Corrected experimental value	$\sigma_N^{\bar{\nu}}/\sigma_N^{\nu}$ Expected value
$V-A$	0.61 ± 0.25	0.38
V or A	0.40 ± 0.17	1.00
$V+A$	0.37 ± 0.16	2.65
S or P or S,P mixture	0.26 ± 0.09	1.00
S,P interference with T	0.31 ± 0.11	1.00
T	0.45 ± 0.15	1.00

$R^{\bar{\nu}}(E_H>0) \equiv \sigma_N^{\bar{\nu}}/\sigma_C^{\bar{\nu}} = 0.33 \pm 0.09$.[28]

More generally, the effective Lagrangian for neutral-current interactions may be written in the quark-parton model as[29]:

$$L = \frac{-G}{\sqrt{2}} \bar{\nu}\gamma_\lambda(1+\gamma_5)\nu \times \{\tfrac{1}{2}[\bar{u}\gamma_\lambda(V_3+A_3\gamma_5)u - \bar{d}\gamma_\lambda(V_3+A_3\gamma_5)d] + \tfrac{1}{2}[\bar{u}\gamma_\lambda(V_1+A_1\gamma_5)u + \bar{d}\gamma_\lambda(V_1+A_1\gamma_5)d]\}, \quad (12)$$

where V_3, A_3, V_1, and A_1 are, respectively, the coupling constants of isovector-vector, isovector-axial-vector, isoscalar-vector and isoscalar-axial-vector currents, and the interactions of $s\bar{s}$, etc., quarks are neglected. In this notation, the overall strength of the weak hadronic neutral current relative to the charged current is

$$\sigma_+ \equiv \frac{\sigma_N^{\nu}+\sigma_N^{\bar{\nu}}}{\sigma_C^{\nu}+\sigma_C^{\bar{\nu}}} = \tfrac{1}{4}(V_3^2+A_3^2+V_1^2+A_1^2) = 0.30 \pm 0.05. \quad (13)$$

Further, the vector-axial-vector interference is measured by

$$\sigma_- \equiv \frac{\sigma_N^{\nu}-\sigma_N^{\bar{\nu}}}{\sigma_C^{\nu}-\sigma_C^{\bar{\nu}}} = \tfrac{1}{2}(V_3A_3+V_1A_1) = 0.26 \pm 0.14. \quad (14)$$

The ratio $\sigma_-/\sigma_+ = 0.87 \pm 0.35$, where we expect +1 for $V-A$ or $A-V$ interference, 0 for pure V or pure A, and -1 for $V+A$ interference.

The inequality of σ_N^{ν} and $\sigma_N^{\bar{\nu}}$ requires the presence of both V and A components in the interaction. In the conventional model, where the interaction is carried by a single W^0, this requires that the weak neutral current be parity violating. It is possible, nonetheless, to construct models of the neutral current which would contain both V and A currents and V,A interference terms and still be parity conserving.[30] Direct observation of parity violation in ν interactions requires measurement of a nonzero pseudoscalar quantity which has not been accomplished as yet in either charged- or neutral-current ν interactions. Direct observation of parity violation is in principle possible in the atomic physics experiments which measure the scattering of polarized light by heavy atoms, although to date those experiments exhibit a null effect.[31]

The results of the experiment described here and those of other recent measurements[6,11] are in agreement. Our measurements of σ_N/σ_C for ν and $\bar{\nu}$ are compared with those of the Gargamelle experiment[11] in Fig. 12. Within errors, the ratios are constant, implying an approximately linear rise of σ_N^{ν} and $\sigma_N^{\bar{\nu}}$ with energy and a diagonal form for the neutral current.[32] The overall relative strength of the neutral current obtained in Eq. (13), 0.30 ± 0.05, is in good agreement with the value obtained in the Caltech-Fermilab experiment,[6] 0.30 ± 0.045.

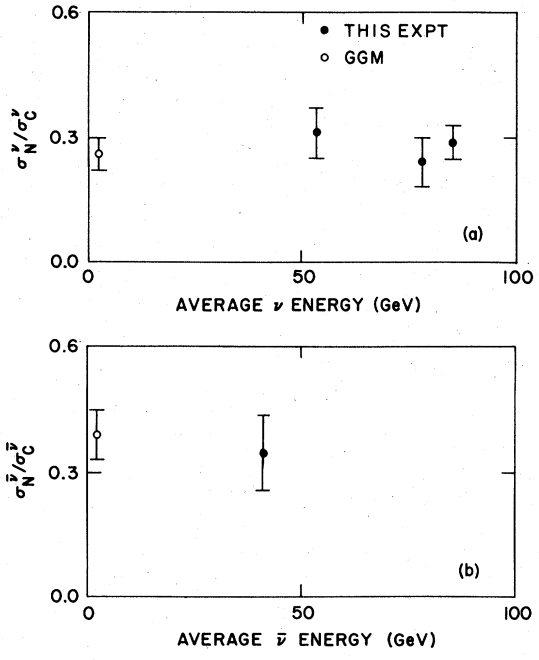

FIG. 12. The ratio of the total neutral-current cross section to the total charged-current cross section for (a) neutrinos and (b) antineutrinos is shown as a function of average beam energy for this experiment and for the Gargamelle experiment (Ref. 11). The total cross sections include contributions from events with low hadron energy which are not detected in the experiments. These contributions are obtained by calculation as discussed in the text.

B. Distribution in hadron energy

The structure of the neutral current can be determined by comparing the measured distribution $d\sigma_N/dE_H$ with that expected for different forms of the neutral current. This determination is independent of the charged-current cross sections, since the uncertainty in the calculation of the muon detection efficiency ϵ_μ is small. It is also independent of the behavior of the neutral-current cross section for $E_H < 4$ GeV.

The measured distributions dN/dE_H for the QT 380 ν data and for the double-horn $\bar{\nu}$ data are compared with several possible forms for these distributions in Figs. 13 and 14. The calculated distributions were obtained by folding the y distribution with the spectra shown in Fig. 4, for the appropriate mixture of ν and $\bar{\nu}$ (Fig. 15). For the QT 380 data, the distributions calculated for S and

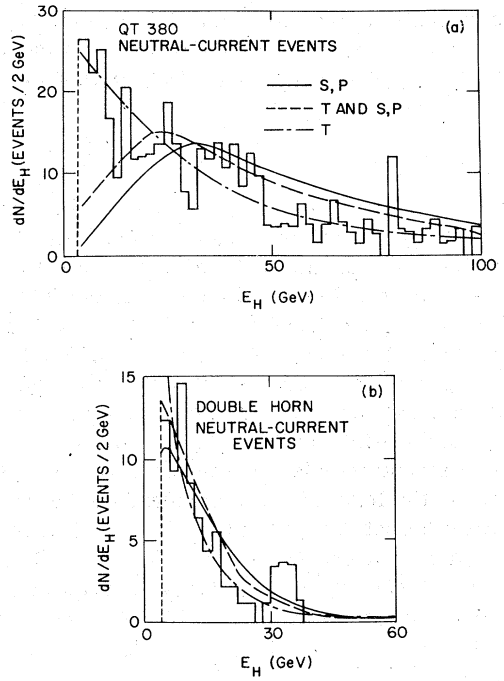

FIG. 13. The measured hadron-energy distributions for neutral-current events are compared with those expected for neutral currents which are pure T, which are S,P admixtures, and which contain T–S,P interference terms, (a) for the largely ν QT 380 run and (b) for the largely $\bar{\nu}$ DH run. The calculated distributions have been normalized to the measured number of events.

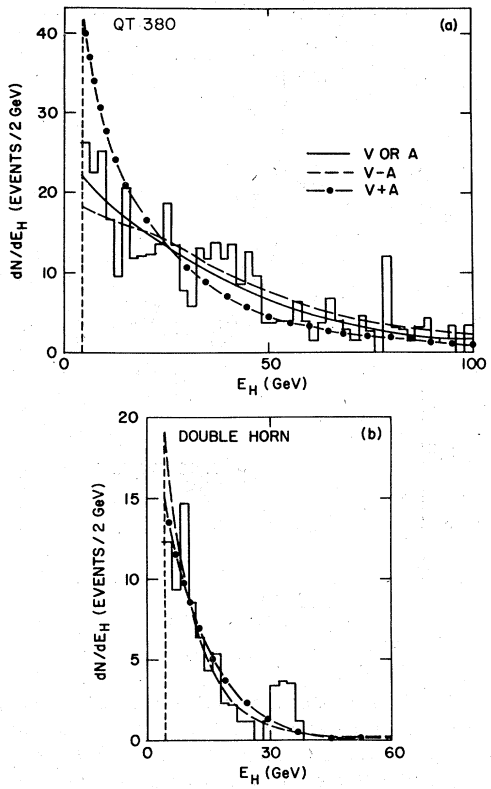

FIG. 14. The measured hadron energy distributions of neutral-current events are compared with those expected for neutral currents which are pure V or pure A, $V-A$, or $V+A$ in form, (a) for the largely ν QT 380 run and (b) for the largely $\bar{\nu}$ DH run. The calculated distributions have been normalized to the measured number of events.

P mixtures, for T interference with S and P, and for $V+A$ currents are much different in shape than the measured distributions. Both $V-A$ and pure V or pure A forms are consistent with the measured distributions. As with $V-A$, $d\sigma/dy$ for a pure T neutral current falls with increasing y; consequently, it is not excluded by the E_H data. The comparisons made in Figs. 13 and 14 give a neutral-current structure that is consistent with the structure obtained from the ratio $\sigma_N^{\bar{\nu}}/\sigma_N^{\nu}$. We have not fitted a form for the neutral current to the E_H distributions for the QT 380 data and the double horn data simultaneously because, when the error in the relative normalization of the ν and $\bar{\nu}$ fluxes is taken into account, the uncertainty in the fit is large enough that it does not distinguish between the various possible neutral-current forms.

C. Model comparisons

The ratios R^{ν} and $R^{\bar{\nu}}$ are compared with the predictions of the Weinberg-Salam model in Fig. 16. Each ratio $R^{\nu}(E_H>0)=\sigma_N^{\nu}/\sigma_C^{\nu}$ and $R^{\bar{\nu}}(E_H>0)=\sigma_N^{\bar{\nu}}/\sigma_C^{\bar{\nu}}$ independently determines a value for $\sin^2\theta_W$. From Fig. 16, R^{ν} gives $\sin^2\theta_W=0.23\pm0.06$. A similar

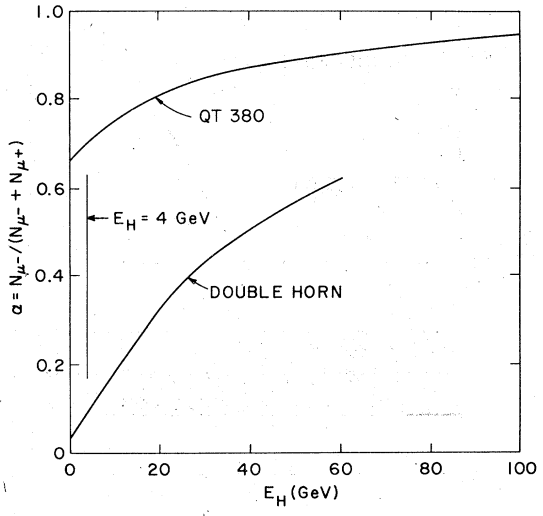

FIG. 15. The parameter α, which gives the ν content of the mixed beams, is plotted against hadron energy E_H for two of the runs. The acceptance cutoff in E_H is also shown. For the QT 380 beam, the average value of α is 0.86. For the DH beam, where the flux falls rapidly for $E_{\bar{\nu}}>10$ GeV, $\langle\alpha\rangle=0.27$.

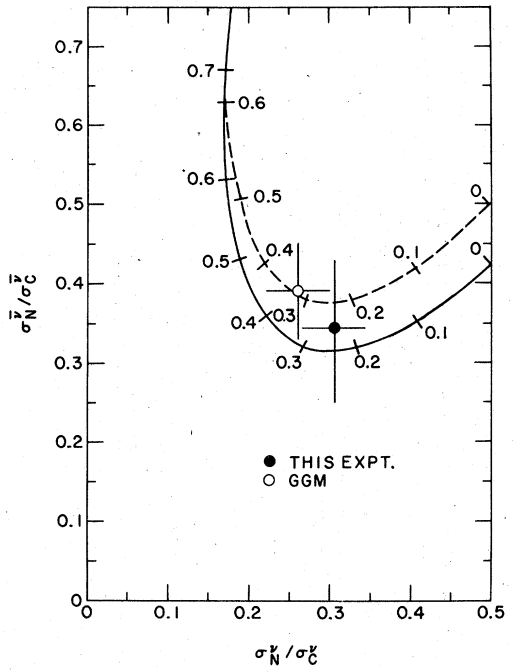

FIG. 16. The ratios of the neutral-current to charged-current cross sections of ν and $\bar{\nu}$ as determined in this experiment and in the Gargamelle experiment (Ref. 11) are compared with the Weinberg-Salam theory. The results of this experiment are to be compared with the solid line, which takes into account the rise in $\sigma_C^{\bar{\nu}}/\sigma_C^{\nu}$ with energy. The results of the Gargamelle experiment are to be compared to the dashed curve, where $\sigma_C^{\bar{\nu}}/\sigma_C^{\nu}$ is constant with energy. The numbers along the curves indicate values of $\sin^2\theta_W$.

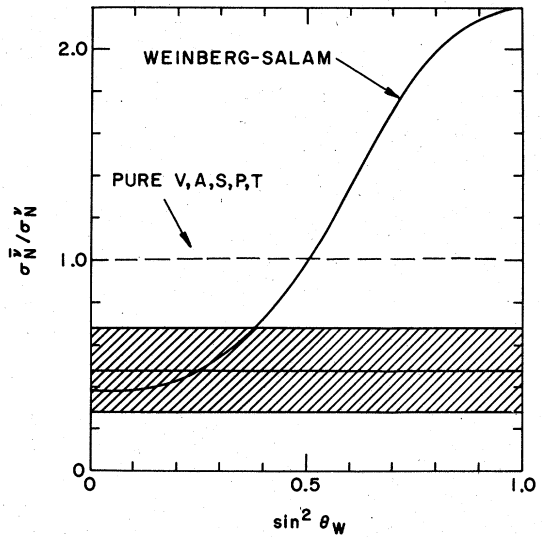

FIG. 17. The ratio $\sigma_N^{\bar{\nu}}/\sigma_N^{\nu}$ and its error are indicated by the central horizontal line and the cross-hatched area. The datum is compared with the value expected if the neutral current has a pure V,A,S,P,T form and with the prediction of the Weinberg-Salam model.

value of $\sin^2\theta_W$ is obtained from $R^{\bar{\nu}}$. In Fig. 17, the data are compared with the Weinberg-Salem theory in a way that is independent of the coupling constant of the neutral current.

VI. CONCLUSIONS

From measurements of neutrino and antineutrino deep-inelastic scattering, we have determined the overall strength of the weak hadronic neutral current relative to the charged current to be (0.30 $\pm$ 0.05). The space-time structure of the neutral current is best fitted by the form $V-(0.7\pm0.3)A$. Our results are also consistent with a $V-A$ form for the neutral current, but are inconsistent with $V+A$, combinations of S and P, or with the presence of strong interference terms between S, P, and T. At the level of three standard deviations, they discriminate against pure V, A, or T forms. For present conventional theories of the weak interaction, these experimental results require a significant parity violating component of the weak neutral current. The corrected ratios of total cross sections are

$$R^{\nu}(E_H>0)\equiv\sigma_N^{\nu}/\sigma_C^{\nu}=0.30\pm0.04\,,$$

$$R^{\bar{\nu}}(E_H>0)\equiv\sigma_N^{\bar{\nu}}/\sigma_C^{\bar{\nu}}=0.33\pm0.09\,.$$

Together with the results of other neutrino experiments, the data described here are consistent with a linear dependence of $\sigma_N^{\bar{\nu}}$ and σ_N^{ν} on neutrino energy. In the context of the Weinberg-Salam gauge theory, these data yield $\sin^2\theta_W=0.23\pm0.06$.

The V, A structure of the weak neutral current obtained here is consistent with the implications of measurements of the electric dipole moments of certain atoms and molecules, which limit the strength of S, P, or T couplings to 10^{-3} G,[33] and also with calculations of stellar evolution rates, which limit the strength of a tensor current T to <0.07 G.[34]

ACKNOWLEDGMENTS

We are grateful for the conscientious scanning of W. Grant, A. Black and P. Deibig, for the technical work of R. Beck, E. Mayer, L. Thomas, and H. Weedon, for the engineering of the Physical Sciences Laboratory of the University of Wisconsin, and for the continuing assistance and encouragement of the Fermilab staff. We thank E. Paschos for useful discussions. One of us (P.W.) thanks Brookhaven National Laboratory for support during the final phase of this work. This work was supported in part by the U.S. Energy Research and Development Administration and performed at the Fermi National Accelerator Laboratory.

*Now at Brookhaven National Laboratory, Upton, New York 11973.
†Now at Universita di Bologna, Bologna, Italy.
‡Now at Rutgers University, New Brunswick, New Jersey 08903.
§Now at Carnegie-Mellon University, Pittsburgh, Pennsylvania 15213. Submitted in partial fulfillment of the Ph.D. requirements at the University of Pennsylvania.
||Now at University of Colorado, Boulder, Colorado 80309.
¶Now at The Ohio State University, Columbus, Ohio 43210.

[1]G. Myatt, in *Proceedings of the Sixth International Symposium on Electron and Photon Interactions at High Energies, Bonn, 1973,* edited by H. Rollnik and W. Pfeil (North-Holland, Amsterdam, 1974), p. 389; F. J. Hasert *et al.*, Phys. Lett. 46B, 138 (1973); A. Benvenuti *et al.*, Phys. Rev. Lett. 32, 800 (1974); F. J. Hasert *et al.*, Nucl. Phys. B73, 1 (1974).
[2]B. Aubert *et al.*, Phys. Rev. Lett. 32, 1454 (1974).
[3]A. Benvenuti *et al.*, Phys. Rev. Lett. 32, 1457 (1974).
[4]A. Benvenuti *et al.*, Phys. Rev. Lett. 37, 1039 (1976).
[5]B. C. Barish *et al.*, Phys. Rev. Lett. 34, 538 (1975).
[6]F. S. Merritt *et al.*, Report No. CALT 68-601, 1977 (unpublished); M. Holder *et al.*, Phys. Lett. 71B, 222 (1977).
[7]P. Schreiner, in *Proceedings of the International Neutrino Conference, Aachen, 1976,* edited by H. Faissner, H. Reithler, and P. Zerwas (Vieweg, Braunschweig, West Germany, 1977), p. 333; S. J. Barish *et al.*, Phys. Rev. Lett. 33, 448 (1974).
[8]D. Cline *et al.*, Phys. Rev. Lett. 37, 252 (1976); 37, 648 (1976).
[9]W. Lee *et al.*, Phys. Rev. Lett. 37, 186 (1976).
[10]J. Blietschau *et al.*, Nucl. Phys. B114, 189 (1976).
[11]J. Blietschau *et al.*, Nucl. Phys. B118, 218 (1977).
[12]F. Reines, H. S. Gurr, and H. W. Sobel, Phys. Rev. Lett. 37, 315 (1976).
[13]F. Messing, thesis, University of Pennsylvania, 1975 (unpublished).
[14]S. Weinberg, Phys. Rev. Lett. 19, 1264 (1967); 27, 1688 (1972); Phys. Rev. D 5, 1412 (1972); A. Salam and J. C. Ward, Phys. Lett. 13, 168 (1964); see also A. Pais and S. B. Treiman, Phys. Rev. D 6, 2700 (1972).
[15]F. Gürsey and P. Sikivie, Phys. Rev. Lett. 36, 775 (1976).
[16]A. Benvenuti *et al.*, Nucl. Instrum Methods 125, 447 (1975); 125, 457 (1975).
[17]B. Aubert *et al.*, in *La Physique Du Neutrino à Haute Énergie*, proceedings of the Colloquium, Ecole Polytechnique, Paris, 1975, edited by A. Rousset and P. Petiau (CNRS, Paris, 1975), p. 385; A. Benvenuti *et al.*, *ibid.*, p. 397.
[18]R. J. Stefanski and H. B. White, Fermilab Report No. FN 292, 1976 (unpublished). We have considered the possible effects of a spectrum which is enhanced above that calculated by Stefanski and White at low energies. An excess similar to that which may have been observed in the ν horn beam (G. Lynch, private communication) was added to the DH and QT 380 beams. At 7 GeV the ν and $\bar{\nu}$ spectra were enhanced by a factor of 7, with the excess decreasing rapidly to 30% at 25 GeV. If such an excess were present in the DH beam, ~60 charged-current events would have been observed in the interval 4 GeV $< E_H <$ 6 GeV. Only 30 such events were present, and we conclude that we see no evidence for such an excess in the DH beam. In the QT 380 beam, such an excess would not be visible because the E_H spectrum at low energies is dominated by events with $E_\nu > 25$ GeV.
[19]B. Aubert *et al.*, Phys. Rev. Lett. 33, 984 (1974); A. Benvenuti *et al.*, *ibid.* 36, 1478 (1976).
[20]J. D. Bjorken and E. A. Paschos, Phys. Rev. D 1, 3151 (1970).
[21]A fit to the data gave $F_2(x) = 0.55(1-x^2)^5 + 0.38x^{0.6}(1-x^2)^3$.
[22]The charged-current cross sections were
$$(d^2\sigma_C^\nu/dxdy) \propto F_2(x)[b(x) + a(x)(1-y)^2]$$
where $a(x) + b(x) = 1$ and
$a(x) = 0.95$ for $E_{\bar{\nu}} < 30$ GeV
$a(x) = 0.52$ for 30 GeV $< E_{\bar{\nu}} <$ 50 GeV, $x < 0.15$,
$a(x) = 0.95$ for 30 GeV $< E_{\bar{\nu}} <$ 50 GeV, $x > 0.15$,
$a(x) = 0.40$ for 50 GeV $< E_{\bar{\nu}}$, $x < 0.15$,
$a(x) = 0.90$ for 50 GeV $< E_{\bar{\nu}}$, $x > 0.15$.
[23]The probability that a muon would be accompanied by a δ ray was established to be 0.14 ± 0.014 from a scan of muons passing through D2 and the spark chambers further downstream.
[24]The measured values of ϵ_p are expected to be slightly lower than the actual values due to the granularity of the liquid-scintillator container. However, since the spark chamber covered the central 80% of the counter area, the effect of this granularity is quite small.
[25]R. L. Kingsley, F. Wilczek, and A. Zee, Phys. Rev. D 10, 2216 (1974); B. Kayser, G. T. Garvey, E. Fishbach, and S. P. Rosen, Phys. Lett. 52B, 385 (1974); S. Pakvasa and G. Rajasekaran, Phys. Rev. D 12, 113 (1975); J. J. Sakurai, *Neutrinos—1974,* proceedings of the Fourth International Conference on Neutrino Physics and Astrophysics, Philadelphia, edited by C. Baltay (A.I.P., New York, 1974), p. 57.
[26]We neglect the production of single strange particles by the charged current, which is <5% of the total charged-current cross sections.
[27]We have neglected isoscalar contributions which are not $V-A$.
[28]If the value of $\sigma_C^{\bar{\nu}}/\sigma_C^\nu$ were taken as 0.38, the corresponding values of $\sigma_N^{\bar{\nu}}/\sigma_N^\nu$ and $R^{\bar{\nu}}(E_H > 0)$ are 0.44 and 0.35, respectively.
[29]J. J. Sakurai, Report No. UCLA/76/TEP/21, 1976 (unpublished); E. A. Paschos, in *Charm, Color and the J/ψ,* proceedings of the X Recontre de Moriond, Méribel-les-Allues, France, 1975, edited by J. Trân Thanh Vân (CNRS, Paris, 1975), p. 341.
[30]T. H. Fritzsch and P. Minkowski, Nucl. Phys. B103, 61 (1976); L. Wolfenstein, in *Proceedings of the Sixth International Symposium on Lepton and Photon Interactions at High Energies, Bonn, 1973,* edited by H. Rollnik and W. Pfiel (North-Holland, Amsterdam, 1974), p. 613; B. Kayser, Phys. Rev. D 15, 3407 (1977); R. N. Mohapatra and D. P. Sidhu, Phys. Rev. Lett. 38, 667 (1977).
[31]L. L. Lewis *et al.*, Phys. Rev. Lett. 39, 795 (1977); P. E. G. Baird *et al.*, *ibid.* 39, 798 (1977).
[32]E. A. Paschos, Phys. Rev. D 15, 1966 (1977); S. L. Glashow and S. Weinberg, *ibid.* 15, 1958 (1977).
[33]F. E. Hinds, C. E. Loving, and P. G. H. Sandars, Phys. Lett. 62B, 97 (1976).
[34]P. Sutherland *et al.*, Phys. Rev. D 13, 2700 (1976).